BOILING OF SATURATED WATER ON GROOVED SURFACE

by

Alangar SATHYABHAMA*

Department of Mechanical Engineering, National Institute of Technology Karnataka, Surathkal, Srinivasnagar Post, Mangalore, India

Original scientific paper
https://doi.org/10.2298/TSCI180105203S

The flow patterns and pool boiling heat transfer performance of rectangular grooved surface immersed in saturated water were experimentally investigated. The effect of the aspect ratio (groove depth/fin thickness) on boiling performance was examined. The test surfaces were manufactured on a copper block with a base diameter of 19 mm with four fin thickness (0.5 mm, 1 mm, 1.5 mm, and 2 mm) and three groove depths (1.0 mm, 2.0 mm, and 3.0 mm). All experiments were performed in the saturated state at atmospheric pressure. A plain surface was used as the reference standard and compared with the grooved surfaces. The photographic images showed different boiling flow patterns among the test surfaces at various heat fluxes. The test results indicated that closer and more number of grooves yielded a greater flow resistance against the bubble/vapour lift-off along the groove wall. At higher heat flux, numerous vapour mushrooms periodically appeared from the perimeter of the grooves. The developed correlation for Nusselt number predicts the experimental data with mean absolute error of 7.42%.

Key words: *aspect ratio, rectangular groove, Nusselt number, bubble frequency, bubble departure diameter*

Introduction

The electronics industry has reduced chip sizes and increased the concentration of the circuits and number of transistors in a silicon chip. Advances in chip design have also increased the power dissipated in a small volume. Higher operating temperature and power consumption by today's electronic components necessitate improved heat transfer from these devices. Boiling heat transfer, a highly efficiency technique, which provides a heat transfer coefficient that is two orders of magnitude higher than that of single phase heat transfer is proposed by several researchers. To reduce the boiling hysteresis and increase the critical heat flow (CHF), enhancement of boiling heat transfer is recommended. The method that has been studied extensively to improve pool boiling heat transfer is small-scale surface enhancement using a variety of techniques, including surface roughening, porous metallic coatings, microporous coatings, microelectromechanical systems fabrication, and others. Several active studies have dealt with the enhancement of boiling heat transfer from electronic components by use of surface microstructures that were fabricated directly on a silicon chip or on a simulated chip. Messina and Park [1], used photographic method for the manufacture of precise arrays of artificial pits on flat plate copper heat transfer surfaces. Anderson and Mudawar [2], employed various arrangements of fins, studs, grooves, and vapor-trapping cavities. Oktay [3]

* Corresponding author, e-mail: bhama72@gmail.com

applied novel surface treatments to large-scale integrated (LSI) devices. Oktay and Schmekenbecher, [4] produced a brush-like heat exchanging structure of ferro-magnetic powder on a semiconductor device chip. Hwang and Moran [5] studied cavities of 3-15 μm mouth diameters drilled by laser over a vertical silicon test surface. Phadke *et al.* [6] produced heat sink surface consisting of a large array of pyramidal cavities etched into the silicon using standard microelectronic fabrication techniques. Kubo *et al.* [7] developed treated surfaces with micro-reentrant cavities by use of microelectronic fabrication techniques. Wright and Gebhart [8] tested micro-configured (hexagonal dimples and rectangular trenches) etched silicon surfaces. Porous surface structure was manufactured with precision by Nakayama *et al.* [9]. Treated surfaces and surface microstructures by spraying and painting were generated by O'Connor *et al.* [10, 11]. Micro-porous enhanced structure was achieved by applying copper and aluminum particle coatings by Chang and You [12]. Bergles and Chyu [13] used commercial porous metallic matrix surface. Thanigaivelan and Deepa [14] aimed to improve the convective heat transfer coefficient by applying aluminum paint coating on a micro-fin structure. The paint coated copper test piece produced 20.62% higher heat transfer compared to aluminum test piece. Meikandan *et al.* [15] investigated the effect of the nanocoating on the heat exchanger surface. The 24.2% improvement in heat transfer rate was observed and transient temperature response of the nanocoated heat exchanger tube is higher than uncoated one for a given experimental conditions.

Several theoretical and experimental studies have been carried out involving pool boiling from single fin or extended surfaces, on both micro- and large-scales. Siman-Tov [16] found that heat transfer performance on a fin array could not be understood by analysing a single fin. Klein and Westwater [17] experimentally analysed transverse fins and cylindrical spins boiling in R-113 and water. Hirono *et al.* [18] proposed that interference between adjacent rectangular fins could reduce the boiling heat transfer performance in the high heat flux region. Guglielmini [19, 20] studied the effects of orientation and geometrical configuration on extended surface and found that straight fin surfaces offered better boiling performance than plane surface. Rainey and You [21] studied the plain and microporous, square pin-finned surfaces. Zhang and Shoji [22] examined the physical mechanisms of the interaction between nucleation sites, and found that it was governed by three factors: hydrodynamic interaction between bubbles, thermal interaction between nucleation sites, and horizontal and declining bubble coalescences. Shoji and Takagi [23] employed a single artificial cavity to analyze the non-linear behaviour and low dimensional chaos of the bubbles. Honda and Wei [24] obtained considerably greater heat transfer from silicon chips with the micropin-fin. Yu *et al.* [25] presented boiling performance and flow mechanism on artificial micro-cavity surfaces with different geometric parameters.

The pool boiling mechanism is very complex and many factors are responsible for high heat transfer rates, including latent heat transfer, natural convection and micro-convection. Several investigators have used visualization as a tool to observe the relative contributions of those mechanisms. Nakayama *et al.* [26] used a rectangular channel covered with a thin sheet with pores at a regular pitch and the entire structure was immersed in R-11. Arshad and Thome [27] conducted visualization from similar surfaces to understand the mechanism of boiling inside the channels. Xia *et al.* [28] observed that the boiling hysteresis attenuates as narrow channels and the first local bubble site is active on the upper part of the narrow channel.

The purpose of the present study is to explore the possibility of enhancing the boiling heat transfer using grooves especially at high heat fluxes. Another main goal of this study is to observe the bubble flow mechanisms of the grooved surface by recording videos.

Experimental apparatus

An experimental facility was designed and constructed to investigate the boiling phenomenon with water as working fluid at atmospheric pressure. The pool boiling experimental apparatus is schematically depicted in fig. 1. The major parts of the test rig are, boiling chamber, heating block, measurement, data acquisition system, and pressure control system. The boiling chamber is a stainless steel square vessel of 200 mm side, 350 mm height, with two circular glass windows, to enable the flow visualisation. The cooling water condenser was coiled in the upper section inside the vessel and connected to a cooling water circulating pump to keep the vessel at atmospheric pressure. A pressure transducer was located at the top of the vessel to measure the pool pressure. The liquid bulk temperature, T_{sat}, and vapour temperature, T_v, were measured using thermocouples. An auxiliary heater of 500 W capacity was inserted into the vessel to heat the liquid bulk to saturation temperature. The schematic details of the heating block are shown in fig. 2, which includes a replaceable test surface mounted on a copper cylindrical rod wrapped with nylon insulator. The 19 mm diameter 7 mm thick circular test surface has a 15 mm diameter 3 mm thick groove which exactly fits on the 15 mm diameter heater rod. To reduce thermal contact resistance between the test surface and the heater rod, thermal grease is used. Resistance heater of 500 W capacity was inserted into the copper rod. All test surfaces used were manufactured by milling grooves on 15 mm diameter 7 mm thick copper piece, as shown in fig. 3. The detailed geometry specifications of grooved surfaces are listed in tab. 1. Three K-type sheathed thermocouples (T_1, T_2, and T_3) of 1 mm diameter are inserted into the holes drilled along the axis of the rod close to the test surface as shown in fig. 2, to calculate the heat flux and the surface temperature. Two K-type sheathed thermocouples, T_4 and T_5, of 1 mm diameter are inserted into the holes drilled in the insulation

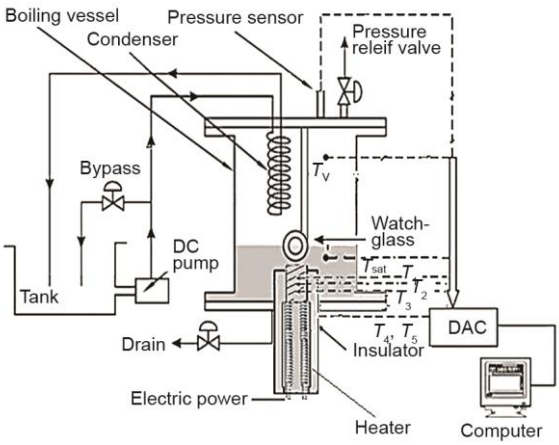

Figure 1. Schematic of test facility T_1, T_2, and T_3 – thermocouples on the copper rod, T_{sat} – thermocouple in the liquid pool, T_v – thermocouple in the vapour region, T_4, T_5 – thermocouples in the insulation

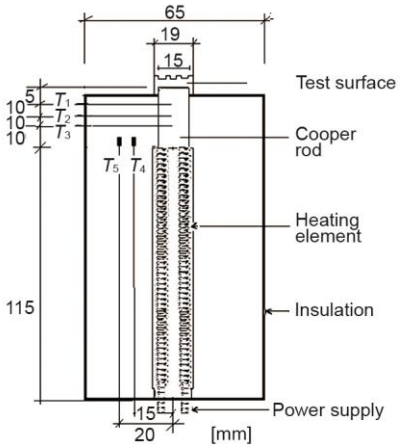

Figure 2. Details of test heater T_4, T_5 – thermocouples in the insulation

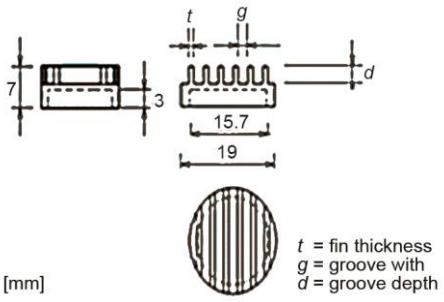

Figure 3. Grooved surface

to calculate the radial heat loss. All the signals, including those from thermocouples, heaters and the pressure transducer were collected by a data acquisition device. A high speed camera (Promon 501) was installed in front of the glass window to observe the mechanism of boiling from these test surfaces. The image was recorded and the data collected simultaneously during the experiment, to enable visual images to be compared with corresponding measurements.

Experimental procedures

The working liquid water was filled into the boiling chamber before the test run and was maintained constant for all the trials. The water was heated to the saturation temperature using auxiliary heater and was boiled vigorously for two hours to remove dissolved gases and any non-condensed gas before the test run. Heat input was given to test heater and after the steady-state was reached, the thermocouple readings were noted down. The power input was increased in small steps and for each steady-state the thermocouple readings were noted down. Meanwhile, the videos were recorded using a camera.

Table 1. Geometrical parameters for rectangular grooved surfaces

Surface type	Groove width, g [mm]	Fin thickness, t [mm]	Groove depth, d [mm]	Aspect ratio
Plain				–
GS 1	2	0.5	3	6
GS 2	2	1.5	3	2
GS 3	2	2	3	1.5
GS 4	2	1	2	2
GS 5	2	1	1	1

Data reduction

The surface temperature of the test piece was calculated by extrapolating the temperature readings obtained from the three thermocouples provided along the length of the heater rod at a distance of 10 mm each. These thermocouple readings were also used to calculate the temperature gradient, dT/dx, and then the heat flux, q, assuming 1-D steady-state heat transfer in the axial direction. Local heat transfer coefficient between the surface and the water was calculated by applying Newton's law of cooling as in eq. (1).

$$h = \frac{q}{\Delta T} = \frac{q}{T_w - T_{\text{sat}}} \quad \text{where} \quad q = k\frac{\mathrm{d}T}{\mathrm{d}x} \tag{1}$$

where T_{sat} is the saturation temperature of the water at the corresponding pressure, T_w – the surface temperature of the test surface, and k – the thermal conductivity of material of heater rod.

To determine bubble departure diameter, the suitable image taken from the recorded videos is processed in MATLAB image processing tool. Here bubble diameter is obtained as pixels. The pixel size of reference object (for example fin thickness) of known size is measured. This is used to find out the conversion factor. Thus, diameter of bubble [mm] is calculated by using eq. (2).

$$d_{\mathrm{b}} = \frac{d_x t}{t_x} \tag{2}$$

where d_{b} is the bubble diameter measured as pixels, t – the known value of thickness taken as reference, and t_x – the reference thickness measured in pixels. One bubble cycle is the sum of the bubble growth period and the waiting period. Bubble cycle for thirty bubbles from the same nucleation site was measured and the average value was determined. The bubble frequency is the reciprocal of this average bubble cycle period.

The uncertainty in temperature measurement is ±0.1 °C. Uncertainty in distance measurement is ±0.1 mm. Kline and McClintock [29] method was used to estimate the uncertainty for the derived quantities.

The uncertainty in wall superheat, heat flux and heat transfer coefficient are calculated by eqs. (3)-(5) respectively.

$$\omega_{\Delta T} = \sqrt{\left(\frac{\omega_{T_w}}{T_w}\right)^2 + \left(\frac{\omega_{T_{\mathrm{sat}}}}{T_{\mathrm{sat}}}\right)^2} \tag{3}$$

$$\omega_q = \sqrt{\left(\frac{\omega_{\mathrm{d}T}}{\mathrm{d}T}\right)^2 + \left(\frac{\omega_{\mathrm{d}x}}{\mathrm{d}x}\right)^2} \tag{4}$$

$$\omega_h = \sqrt{\left(\frac{\omega_q}{q}\right)^2 + \left(\frac{\omega_{\Delta T}}{\Delta T}\right)^2} \tag{5}$$

The resulting maximum uncertainty in the heat flux was 1.55%. The maximum uncertainty in the wall superheat values was 0.44%. The maximum uncertainty in the heat transfer coefficient was 2.57%.

Results and discussion

The plot presented in fig. 4 illustrates the typical boiling curve for various grooved surfaces. It is clear that grooves improve the heat transfer. An attempt is made to establish the effect dimensionless parameter, aspect ratio (groove depth/fin thickness) on heat transfer. It may be observed that there are not any clear trends that result from creating dimensionless parameter. This implies that the heat transfer capabilities are dependent on the absolute dimensions of the groove geometry in the present work. For example, GS2 and GS4 have similar aspect ratio values of 2, but the two surfaces are drastically different in regard to heat dissipation. Therefore, in this current work, the effectiveness of the grooved surfaces cannot be classified based on the dimensionless quantity. This is in contrast to Yu and Lu [30], who observed that the fin aspect ratio strongly affects the CHF enhancement, because, lower aspect ratio fins, either lower fin length or larger fin spacing, provide lower resistance to the departure bubble and re-wetting liquid and yield higher heat transfer rate per unit area.

Figure 5 shows the variation of bubble departure diameter with heat flux for different surfaces. Bubble departure diameter increases initially with increase in heat flux, then it drops sharply at higher heat flux for grooved surfaces. This shows that surface tension is dominant force for grooved surfaces. Frequency of bubble formation as a function of heat flux for different surfaces is depicted in fig. 6. The results show that the frequency of bubble generation increases with heat flux and is higher for grooved surfaces compared to the plain surface. This results in higher heat transfer from grooved surfaces.

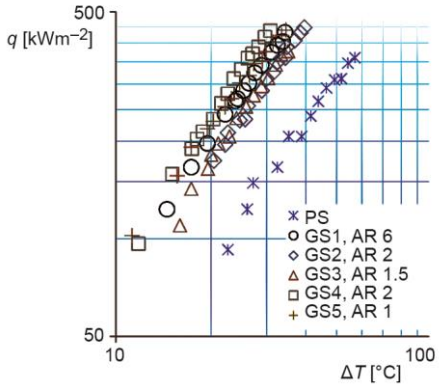

Figure 4. Boiling curves for different surfaces

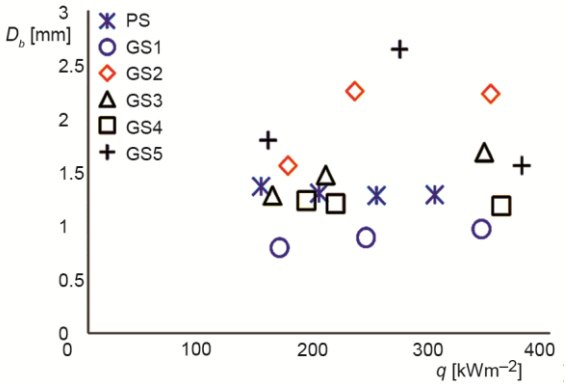

Figure 5. Bubble departure diameter *vs.* heat flux

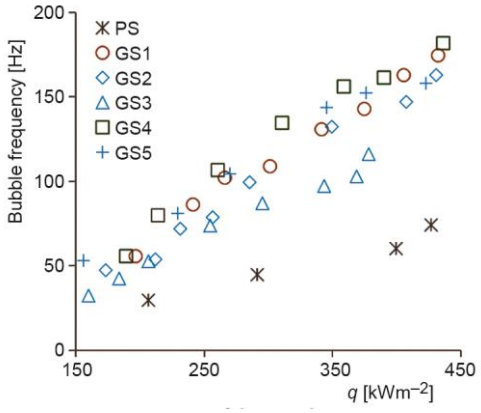

Figure 6. Bubble frequency *vs.* heat flux

Visualisation of boiling on surfaces

The videos recorded during experimentation are converted into images and are used to study the effect of groves on bubble dynamics. At low heat flux, few bubbles formed from active nucleation sites on the grooves and the remaining portion was under free convection as shown in figs. 7(a)-7(c). The bubbles always originated from some fixed sites, the groove corner and slid along the channel wall. The channels were always flooded with liquid and the liquid meniscus can be seen. The liquid that is getting heated up on the fin top from adjacent fins form huge bubble over the liquid meniscus. At higher heat flux, more number of bubbles are formed and bubble coalescence can be observed between the adjacent channels as observed from figs. 7(d)-7(f).

Correlation development

The pool boiling heat transfer depends on the parameters density, ρ, specific heat, C_p, latent heat, h_{fg}, heat flux, q, wall superheat, ΔT, thermal conductivity, k, bubble departure diameter, d_b, and frequency, f. For grooved surface additional geometric parameters, groove width, g, fin thickness, t, and groove depth, d, are considered. The parameters and properties

are grouped to form dimensionless numbers by Buckingham's π-theorem and seven π-terms are obtained. These π-terms are:

$$\pi_1 = \frac{g}{t}, \pi_2 = \frac{d}{t}, \pi_3 = \frac{\rho^{2/3} h_{fg}}{q''^{2/3}}, \pi_4 = \frac{\rho^{1/3} tf}{q''^{1/3}}, \pi_5 = -\frac{d_b}{t}, \pi_6 = \frac{\rho^{2/3} \Delta T C_p}{q''^{2/3}}, \quad \text{and} \quad \pi_7 = \frac{\Delta T k}{tq''}$$

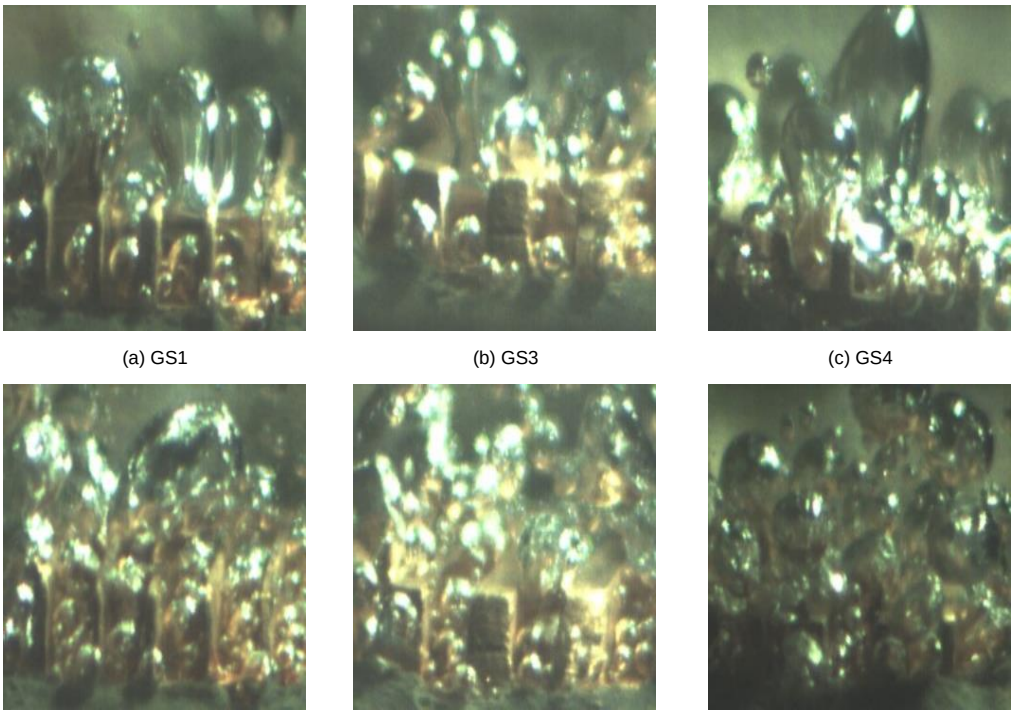

(a) GS1 (b) GS3 (c) GS4

(d) GS1 (e) GS3 (f) GS4

Figure 7. Flow patterns on grooved surfaces; (a)-(c) q = 90 kW/m^2, (d)-(f) q = 300 kW/m^2

The dimensionless number π_7 can be expressed as a function of other π-terms as shown in eq. (6). The power law regression method is used to obtain the correlation between π_7 and other π-terms. The correlation obtained is as shown in eq. (7):

$$\pi_7 = f(\pi_1, \pi_2, \pi_3, \pi_4, \pi_5, \pi_6) \tag{6}$$

$$\frac{\Delta T k}{tq''} = 0.0988 \left(\frac{g}{t}\right)^{0.2993} \left(\frac{d}{t}\right)^{0.2812} \left(\frac{\rho^{2/3} h_{fg}}{q''^{2/3}}\right)^{0.0325} \left(\frac{\rho^{1/3} tf}{q''^{1/3}}\right)^{-0.02381} \left(\frac{d_b}{t}\right)^{0.1218} \left(\frac{\rho^{2/3} \Delta T C_p}{q''^{2/3}}\right)^{-0.0898} \tag{7}$$

In eq. (7) $(\Delta Tk)/(tq'')$ can be represented as $k/(th)$, where $h = q''/\Delta T$ and $k/(th) = 1/\mathrm{Nu}$.

The final expression for Nusselt number is as given by eq. (8):

$$\mathrm{Nu} = 10.1215\left(\frac{t}{g}\right)^{0.2993}\left(\frac{t}{d}\right)^{0.2812}\left(\frac{q''^{2/3}}{\rho^{2/3}h_{fg}}\right)^{0.0325}\left(\frac{q''^{1/3}}{\rho^{1/3}tf}\right)^{-0.02381}\left(\frac{t}{d_\mathrm{b}}\right)^{0.1218}\left(\frac{q''^{2/3}}{\rho^{2/3}\Delta TC_p}\right)^{-0.0898} \tag{8}$$

The mean absolute error (MAE) of Nusselt number calculated from the experiment and those predicted from the present correlation is obtained using eq. (9) and it is plotted in fig. 8. The MAE is found to be 7.42% in the investigated range of heat flux.

$$MAE = \frac{1}{n}\sum\left(\frac{\text{theoretical values} - \text{experimental values}}{\text{theoretical values}}\right)\cdot 100 \tag{9}$$

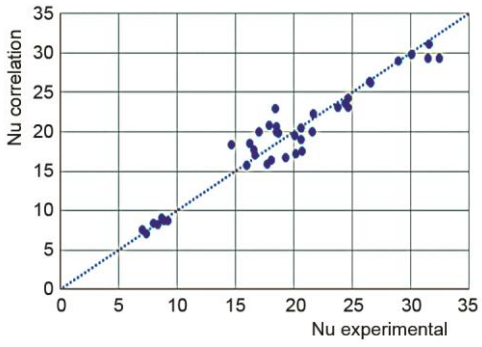

Figure 8. Error analysis

Conclusions

Pool boiling heat transfer from plain and grooved surfaces immersed in saturated water at atmospheric pressure was experimentally studied. The effects of aspect ratio on the nucleate boiling heat transfer performance were also reported. Visualisation studies were done to ascertain the cause for enhancement in heat transfer from grooved surfaces. The experimental results support the following conclusions.

- Boiling generally initiated at the base of the groove, it spread to the fin root, regardless of the heat flux. This result was associated with the fact that generated bubbles can be easily eliminated by the capillary action.
- Large vapour mushroom clouds were found to accumulate inside the channel, at high heat flux.
- The enhancement of heat transfer rate was not proportional to the total aspect ratio.
- Prediction accuracy of developed correlation for Nusselt number was 7.42%

Acknowledgment

Authors would like to acknowledge the financial support extended by the Council of Scientific and Industrial Research (CSIR), India, (sanction order 22/661/14/EMR-II) to carry out this research work.

Nomenclature

C_p – specific heat, [Jkg^{-1}K^{-1}]
d – groove depth, [m]
d_b – bubble departure diameter, [m]
f – bubble frequency, [Hz]
h – heat transfer coefficient, [Wm^{-2}°C^{-1}]
h_{fg} – latent heat of vaporization, [Jkg^{-1}]
k – thermal conductivity, [Wm^{-1}K^{-1}]
Nu – Nusselt number, [–]
q – heat flux, [Wm^{-2}]
T – temperature, [°C]
ΔT – temperature difference, [°C]
t – fin thickness, [m]
w – groove width, [m]

Greek symbol

ρ – density, [kgm^{-3}]

References

[1] Messina, A. D., Park, E. L., Jr., Effects of Precise Arrays of Pits on Nucleate Boiling, *Internacional Journal of Heat and Mass Transfer, 24*, (1981), 1, pp. 141-145
[2] Anderson, T. M., Mudawwar, I., Microelectronic Cooling by Enhanced Boiling of a Dielectric Fluorocarbon Liquid, *Journal of Heat Transfer, 111* (1989), 3, pp. 752-759
[3] Oktay, S., Departure from Natural Convection (DNC) in Low-Temperature Boiling Heat Transfer Encountered in Cooling Micro-Electronic LSI Devices., *Proceeding* 7th International Heat Transfer Conference, Munich, Germany, (1982), Vol. 4, pp. 113-118
[4] Oktay, S., Schmekenbecher, A., Method for Forming Heat Sinks on Semiconductor Device Chips, U. S. Patent No. 3706127, 1972
[5] Hwang, U. P., Moran, K. F., Boiling Heat Transfer of Silicon Integrated Circuits Chip Mounted on a Substrate., *Heat Transfer in Electronic Equipment ASME HTD, 20* (1981), Nov., pp. 53-59
[6] Phadke, N. K., *et al*., Re-Entrant Cavity Surface Enhancements for Immersion Cooling of Silicon Multichip Packages, *IEEE Trans. Components Hybrids Manufacturing Technology, 15* (1992), 5, pp. 815-822
[7] Kubo, H., *et al*., Effects of Size and Number Density of Micro-Re-Entrant Cavities on Boiling Heat Transfer from a Silicon Chip Immersed in Degassed and Gas Dissolved FC-72. *Journal of Enhanced Heat Transfer, 6* (1999), 2, pp. 151-160
[8] Wright, N., Gebhart, B., Enhanced Boiling on Micro-Configured Surfaces, *ASME J. Heat Transfer, 111* (1989), 2, pp. 112-120
[9] Nakayama, W., *et al*., Effects of Pore Diameters and System Pressure on Saturated Pool Nucleate Boiling Heat Transfer from Porous Surfaces, *ASME Journal of Heat Transfer*, *104* (1982), 2, pp. 286-291
[10] O'Connor J. P., *et al*., A Dielectric Surface Coating Technique to Enhance Boiling Heat Transfer from High Power Microelectronics, *IEEE Transactions Components Packaging Manufacturing Technology, 18* (1995), 3, pp. 656-663
[11] O'Connor J. P., *et al*., Gas Saturated Pool Boiling Heat Transfer from Smooth and Microporous Surfaces in FC-72. *ASME Journal of Heat Transfer, 118* (1996), 3, pp. 662-667
[12] Chang, J. Y., You, S. M., Heat Orientation Effects on Pool Boiling of Micro-Porous-Enhanced Surfaces in Saturated FC-72. *ASME Journal of Heat Transfer, 118* (1996), 4, pp. 937-943
[13] Bergles, A. E., Chyu, M. C., Characteristics of Nucleate Pool Boiling from Porous Metallic Coatings, *ASME Journal of Heat Transfer, 104* (1982), 2, pp. 279-285
[14] Thanigaivelan, R., Deepa, D., Heat Transfer Enhancement by Coated Fins in the Microscale Domain, *Thermal Science, 22* (2018), 6B, pp. 2783-2789
[15] Meikandan, M., *et al*., Experimental Investigation on Thermal Performance of Nano Coated Surfaces for Air-Conditioning Applications, Thermal Science, On-line first, https://doi.org/10.2298/TSCI160825 175M
[16] Siman-Tov, M., Analysis and Design of Extended Surfaces in Boiling Liquids, *Chem. Engrg. Progr. Symp. Ser., 66* (1970), pp. 174-184
[17] Klein, G. J., Westwater, J. W., Heat Transfer from Multiple Spines to Boiling Liquids, *AIChE Journal, 17* (1971), 5, pp. 1050-1056
[18] Hirono, Y., *et al*., Optimization of Fin Array in Boiling Heat Transfer, *Technical Report of Tohoku University, 50* (1985), 1, pp. 21-39
[19] Guglielmini, G., *et al*., Experiments on Pool Boiling of a Dielectric Fluid on Extended Surfaces, *International Communications in Heat and Mass Transfer, 23* (1996), 4, pp. 451-462
[20] Guglielmini, G., *et al*., Boiling of Saturated FC-72 on Square Pin Fin Arrays, *International Journal Thermal Science, 41* (2002), 7, pp. 599-608
[21] Rainey, K. N., You, S. M., Pool Boiling Heat Transfer from Plain and Microporous, Square Pin-Finned Surfaces in Saturated FC-72, *ASME Journal of Heat Transfer, 122* (2000), 3, pp. 509-516
[22] Zhang, L., Shoji, M., Nucleation Site Interaction in Pool Boiling on the Artificial Surface, *International Journal in Heat and Mass Transfer, 46* (2003), 3, pp. 513-522
[23] Shoji, M., Takagi, Y., Bubbling Features from a Single Artificial Cavity, *International Journal in Heat and Mass Transfer, 44* (2001), 4, pp. 2763-2776
[24] Honda, H., Wei, J. J., Effects of Fin Geometry on Boiling Heat Transfer from Silicon Chips with Micro-pin-Fins Immersed in FC-72, *International Journal in Heat and Mass Transf, 46* (2003), 21, pp. 4059-4070

[25] Yu, C. K., *et al*., Pool Boiling Heat Transfer on Artificial Micro-Cavity Surfaces in Dielectric Fluid FC-72, *Journal of Micromechanics Microengineering*, *16* (2006), 10, pp. 2092-2099
[26] Nakayama, W., *et al*., Dynamic Model of Enhanced Boiling Heat Transfer on Porous Surfaces Part I: Experimental Investigation, *Journal of Heat Transfer*, *102* (1980), 3, pp. 445-450
[27] Arshad, J., Thome, J. R., Enhanced Boiling Surfaces: Heat Transfer Mechanism and Mixture Boiling, *Proceedings of ASME-JSME Thermal Engineering Joint Conference*, *1* (1983), 1, pp. 191-197
[28] Xia, C., *et al*., Natural Convective Boiling in Vertical Rectangular Narrow Channels, *Experimental Thermal and Fluid Science*, *12* (1996), 3, pp. 313-324
[29] Kline, S. J., McClintock, F. A., Describing the Uncertainties in Single Sample Experiment, *Mechanical Engineering 75*, (1953), 3-8, pp. 3-12
[30] Yu, C. K., Lu, D. C., Pool Boiling Heat Transfer on Horizontal Rectangular Fin Array in Saturated FC-72, *International Journal of Heat and Mass Transfer*, *50* (2007), 17-18, pp. 3624-3637

Paper submitted: January 5, 2018
Paper revised: July 23, 2018
Paper accepted: July 28, 2018